

# Geophysical Research Letters®







## RESEARCH LETTER

10.1029/2023GL104770

### Special Section:

Years of the Maritime Continent

## Cross-Equatorial Surges Boost MJO's Southward Detour Over the Maritime Continent

Sandro W. Lubis<sup>1</sup> , Samson Hagos<sup>1</sup> , Chuan-Chieh Chang<sup>1</sup>, Karthik Balaguru<sup>1</sup> , and L. Ruby Leung<sup>1</sup> 

<sup>1</sup>Pacific Northwest National Laboratory, Richland, WA, USA

### Key Points:

- Cross-equatorial surge (CES) amplifies Madden-Julian oscillation (MJO)'s southward detour during the active Australian monsoon season (December–March)
- Zonal moisture convergence by CES wind acting upon the background moisture increases MJO convection over the southern Maritime Continent
- CES-induced intensification of low-level northwesterly and westerly winds enhances positive wind-evaporation feedback onto MJO convection

### Supporting Information:

Supporting Information may be found in the online version of this article.

### Correspondence to:

S. W. Lubis,  
[sandro.lubis@pnnl.gov](mailto:sandro.lubis@pnnl.gov)

### Citation:

Lubis, S. W., Hagos, S., Chang, C.-C., Balaguru, K., & Leung, L. R. (2023). Cross-equatorial surges boost MJO's southward detour over the Maritime Continent. *Geophysical Research Letters*, 50, e2023GL104770. <https://doi.org/10.1029/2023GL104770>

Received 30 MAY 2023

Accepted 24 JUL 2023

Corrected 21 AUG 2023

This article was corrected on 21 AUG 2023. See the end of the full text for details.

### Author Contributions:

**Conceptualization:** Sandro W. Lubis

**Data curation:** Sandro W. Lubis

© 2023 Battelle Memorial Institute. This is an open access article under the terms of the [Creative Commons Attribution-NonCommercial-NoDerivs License](#), which permits use and distribution in any medium, provided the original work is properly cited, the use is non-commercial and no modifications or adaptations are made.

**Abstract** The influence of the cross-equatorial northerly surge (CES) on the eastward propagation of Madden-Julian oscillation (MJO) during boreal winter is evaluated through the analysis of the column integrated moisture budget. Results show that the CES reinforces MJO's southward detour by increasing horizontal moisture convergence over the southern Maritime Continent (MC) region. Further analysis reveals that the zonal convergence by intraseasonal zonal wind anomalies acting upon background moisture is intensified in the presence of CES events, causing a stronger convective activity in the southern MC (SMC). The stronger moisture convergence in the SMC is associated with the CES-induced intensification of low-level northwesterly and westerly winds, which, in turn, strengthen zonal wind convergences and positive wind-evaporation feedbacks onto the MJO convection. An improved process understanding of the link between the CES and MJO detours can help engender improvements in extreme weather forecasts and aid investigation biases in simulating MJO in climate models.

**Plain Language Summary** Madden-Julian oscillation (MJO) is a tropical large-scale atmospheric phenomenon characterized by an eastward propagating band of clouds and rainfall. Sometimes, during its journey over the Maritime Continent (MC), the MJO takes a southward detour. This detour can have significant impacts on the climate and weather patterns. In this study, we explore the potential impact of a cross-equatorial northerly cold surge (CES) on the magnitude of the MJO detour over the MC. We find that the magnitude of the MJO's southward detour becomes stronger in the presence of CES events. The CES increases northwesterly and westerly winds, which in turn enhances zonal moisture convergence and strengthens positive wind-evaporation feedback onto MJO convection. A better understanding of the relationship between the CES and the MJO can lead to improvements in extreme weather forecasting over the MC and other regions, and aid in investigating biases in simulating MJO propagation in global climate models.

## 1. Introduction

Notwithstanding significant progress made in the past decades on understanding the Madden-Julian oscillation (MJO), many fundamental questions regarding its observed behaviors over the Maritime Continent (MC) remain elusive. One of such aspects is the so-called MJO “detours,” which describe a southward shift of MJO eastward propagation when crossing the MC in boreal winter (Kim et al., 2017; Singh & Kinter, 2020; Zhang & Dong, 2004). Several mechanisms have been proposed to explain the underlying mechanisms of the MJO detour (Kang et al., 2021, 2022; Kim et al., 2017; Zhou & Murtugudde, 2020). For example, Kim et al. (2017) found that the stronger climatological-mean moisture gradients in the southern MC (SMC) relative to the equatorial MC are critical to the southward detour of MJO. On the other hand, Zhou and Murtugudde (2020) argued that warm sea surface temperature anomalies over the SMC prior to the onset of the MJO are important for the southward detour due to enhanced local convection. More recently, Kang et al. (2022) demonstrated that the MJO detour exhibits seasonality and is primarily observed during the Australian monsoon season (December to March, DJFM). This season provides a conducive background state for MJO development in the SMC, which is characterized by a stronger positive wind-evaporation feedback due to the background westerly winds in the lower troposphere. While these studies have proposed some compelling hypotheses, no consensus exists on the factors that govern the magnitude of the southward detour, particularly with regards to the potential role of remote extratropical forcing.

A cross-equatorial northerly cold surge (CES) is a large-scale atmospheric disturbance in the MC region, characterized by a burst of strong northeasterly winds that originate from the high latitudes, and propagate far to

**Formal analysis:** Sandro W. Lubis  
**Funding acquisition:** L. Ruby Leung  
**Investigation:** Sandro W. Lubis, Samson Hagos, Chuan-Chieh Chang, Karthik Balaguru, L. Ruby Leung  
**Methodology:** Sandro W. Lubis  
**Project Administration:** L. Ruby Leung  
**Supervision:** Sandro W. Lubis  
**Visualization:** Sandro W. Lubis  
**Writing – original draft:** Sandro W. Lubis  
**Writing – review & editing:** Sandro W. Lubis, Samson Hagos, Chuan-Chieh Chang, Karthik Balaguru, L. Ruby Leung

the tropical region (Chang et al., 2005; Hattori et al., 2011; Lim et al., 2017; Xavier et al., 2020). It involves the movement of dry cold air outbreaks within the boreal winter monsoon flow, which, as they pass over warm tropical waters, collect considerable amounts of moisture along their trajectory. Furthermore, due to the combined effects of the planetary vorticity gradient, as well as the blocking and deflection caused by topography during the equatorial crossing, the moist low-level air becomes accumulated over the SMC (Chang et al., 2005; Hattori et al., 2011; Lim et al., 2017), leading to intense convection over the region. While cold surges are typically associated with high-frequency wind variability (<20 days) over the South China Sea in November and December, they can also exhibit intraseasonal variations when crossing the equator at the end of January and February (Xavier et al. (2020), see also Figures S1 and S2 in Supporting Information S1). A few studies have also provided evidence that MJO events occurring during CES episodes can enhance deep convection over many regions in the SMC (Hattori et al., 2011; Pang et al., 2018). This finding aligns with other studies showing that when the cold surge and MJO coincides, albeit this occurrence is rare, can produce heavy rainfall over the SMC regions (Abdillah et al., 2021; Lim et al., 2017; Wu et al., 2007; Xavier et al., 2020). However, what is still missing in the current literature is the physical mechanism underpinning the effect of the CES on MJO intensity and propagation.

Considering the significant influence of the CES on circulation and moisture over the SMC and that MJO exhibits sensitivity to background moisture and its gradients, it is plausible to hypothesize that CES may reinforce the magnitude of the MJO southward detour. In this study, we leverage the so-called moisture mode theory of MJO (Sobel & Maloney, 2013), to emphasize the role of moisture in the MJO dynamics during CES events. Then, we seek to further investigate the potential impact of the CES on the wind-evaporation feedback, which is hypothesized to play a critical role in the development of convective activities in MJO over the SMC.

## 2. Data and Methodology

### 2.1. Data Set

We focus on MJO propagation during the active Australian monsoon period (DJFM) using daily outgoing long-wave radiation (OLR) data as a proxy of tropical deep convection from 1979 to 2020 (Liebmann & Smith, 1996). Three-dimensional atmospheric states, including zonal and meridional winds ( $u$  and  $v$ ), vertical velocity ( $\omega$ ), latent heat flux, and specific humidity ( $q$ ) are obtained from the European Centre for Medium-Range Weather Forecasts ERA-5 reanalysis product (Hersbach et al., 2020) from 1979 to 2020. In addition, we also use daily averaged precipitation data from the Integrated Multi-satellite Retrievals for GPM (IMERG) from 2001 to 2020 (Huffman et al., 2020). Daily anomalies are produced by removing the first three harmonics of the annual cycle from all variables. The MJO-filtered anomaly is obtained by retaining only eastward propagating wavenumbers 1–9 and 20–90-day periods using Fourier and inverse-Fourier transform, similar to Wheeler and Kiladis (1999).

### 2.2. MJO Moisture Budget

In moisture mode theory, the processes that lead to moistening during the MJO's propagation can be understood by invoking the vertically integrated intraseasonal moisture budget equation:

$$\frac{\partial \langle q' \rangle}{\partial t} = -\langle \nabla \cdot (\mathbf{V}q) \rangle' - \left\langle \frac{\partial(\omega q)}{\partial p} \right\rangle' - \left\langle \frac{Q_2}{L_q} \right\rangle'; \quad (1)$$

where primes represent intraseasonal anomalies,  $\mathbf{V}$  is the horizontal wind vector,  $\nabla \cdot$  is the divergence operator,  $Q_2$  is the atmospheric apparent moisture loss (gain), and  $L_q$  is the latent heat of condensation. The variables with angle brackets denote a mass-weighted vertical integral:

$$\langle \cdot \rangle = \frac{1}{g} \int_{p_T}^{p_s} (\cdot) dp, \quad (2)$$

with  $p_T = 100$  hPa and  $p_s = 1,000$  hPa. The first term on the right-hand side of Equation 1 represents the total moisture flux convergence, the second term represents the vertical moisture advection in the flux form, and the third term represents moisture loss (gain) due to the condensation/evaporation processes. The total moisture flux

convergence can be decomposed into the horizontal moisture advection and the moisture flux convergence due to convergence of wind:

$$-\langle \nabla \cdot (\mathbf{V}q) \rangle' = -\langle \mathbf{V} \cdot \nabla q \rangle' - \langle q \nabla \cdot \mathbf{V} \rangle'. \quad (3)$$

With negligible storage  $-\partial(\omega q)/\partial p$ , the dominant balance in the moisture budget equation (Eq. 1) is between the total moisture flux convergence  $-\langle \nabla \cdot (\mathbf{V}q) \rangle'$  and the net precipitation  $Q_2/L_q \approx (P - E)$ . Therefore, positive (negative) values of total moisture flux convergence correspond to positive (negative) net precipitation.

The relative contributions of the mean state, intraseasonal anomalies, and high-frequency eddy anomalies are identified by further decomposing each variable into the low-frequency background (>90 days), intraseasonal (20–90 days), and high-frequency (<20 days) components. For example,  $q$  can be decomposed as  $q = \bar{q} + q' + q^*$ . With this decomposition, the horizontal moisture convergence terms in Equation 3 can be partitioned into nine terms as follows (e.g., Hsu and Li (2012)):

$$\begin{aligned} -\left\langle q \frac{\partial u}{\partial x} \right\rangle' &\cong -\left\langle \bar{q} \frac{\partial \bar{u}}{\partial x} \right\rangle' - \left\langle \bar{q} \frac{\partial u'}{\partial x} \right\rangle' - \left\langle \bar{q} \frac{\partial u^*}{\partial x} \right\rangle' - \left\langle q' \frac{\partial \bar{u}}{\partial x} \right\rangle' - \left\langle q' \frac{\partial u'}{\partial x} \right\rangle' \\ &\quad - \left\langle q' \frac{\partial u^*}{\partial x} \right\rangle' - \left\langle q^* \frac{\partial \bar{u}}{\partial x} \right\rangle' - \left\langle q^* \frac{\partial u'}{\partial x} \right\rangle' - \left\langle q^* \frac{\partial u^*}{\partial x} \right\rangle', \end{aligned} \quad (4)$$

$$\begin{aligned} -\left\langle q \frac{\partial v}{\partial y} \right\rangle' &\cong -\left\langle \bar{q} \frac{\partial \bar{v}}{\partial y} \right\rangle' - \left\langle \bar{q} \frac{\partial v'}{\partial y} \right\rangle' - \left\langle \bar{q} \frac{\partial v^*}{\partial y} \right\rangle' - \left\langle q' \frac{\partial \bar{v}}{\partial y} \right\rangle' - \left\langle q' \frac{\partial v'}{\partial y} \right\rangle' \\ &\quad - \left\langle q' \frac{\partial v^*}{\partial y} \right\rangle' - \left\langle q^* \frac{\partial \bar{v}}{\partial y} \right\rangle' - \left\langle q^* \frac{\partial v'}{\partial y} \right\rangle' - \left\langle q^* \frac{\partial v^*}{\partial y} \right\rangle'. \end{aligned} \quad (5)$$

### 2.3. Defining CES and MJO Events

Cold surges are identified based on the criteria proposed by Lim et al. (2017) as days when the average northeasterly wind speed over the South China Sea (5–10°N, 107–115°E, depicted by the blue box in Figure 1a) is exceeding 0.75 standard deviations (equivalent to 2.76 m s<sup>-1</sup>) above the long-term DJFM mean (7.58 m s<sup>-1</sup>). The identified cold surge events are then examined for their equatorial crossing using a definition similar to that of Hattori et al. (2011). Specifically, if the normalized northerly wind speed over 5°S–5°N, 105°–115°E (depicted by the red box in Figure 1a) during a cold surge exceeds one standard deviation (equivalent to 1.95 m s<sup>-1</sup>), then it is classified as a cross-equatorial surge (CES). Using this definition, we identify a total of 472 CES events.

To define individual MJO events, we use a regional OLR index over the East Indian Ocean similar to Kim et al. (2017). This index is calculated based on MJO-filtered OLR anomalies averaged over 15°S–15°N, 70°–100°E. We search for days when the OLR index falls below one negative standard deviation and exhibits continuous eastward propagation for at least 30° longitude. The initial day of each consecutive period that meets this threshold is referred to as day 0. By applying this criteria, we identify a total of 111 MJO events. To investigate the relationship between MJO and CES, we further divide these events into two groups based on whether or not the CES is detected during the MJO eastward propagation over the MC (from day 0 to day 25). The 26-day time window represents the average time it takes the MJO to cross over the MC. Note that the results below are not sensitive when considering a slightly smaller or larger window size (e.g., 20 or 30 days). In total, we identify 38 MJO events with CES (MJO\_CES) and 73 MJO events without CES (MJO\_noCES) for the period of interest. In other words, 34% of the total MJO events involve a CES event, while the remaining 66% do not.

### 2.4. Statistical Significance

A significance test for the composite anomalies is carried out using a bootstrap resampling method (Efron, 1979). We randomly generate 1,000 synthetic composites for MJO\_CES or MJO\_noCES to obtain a sufficiently large sample size, and the 2.5th and 97.5th percentile values are used to define the 95% confidence interval using a two-sided test. To address the sample size imbalance between MJO\_CES and MJO\_noCES, we randomly select, with replacement, an equivalent number of days from the MJO\_noCES to match the number of MJO\_CES events.

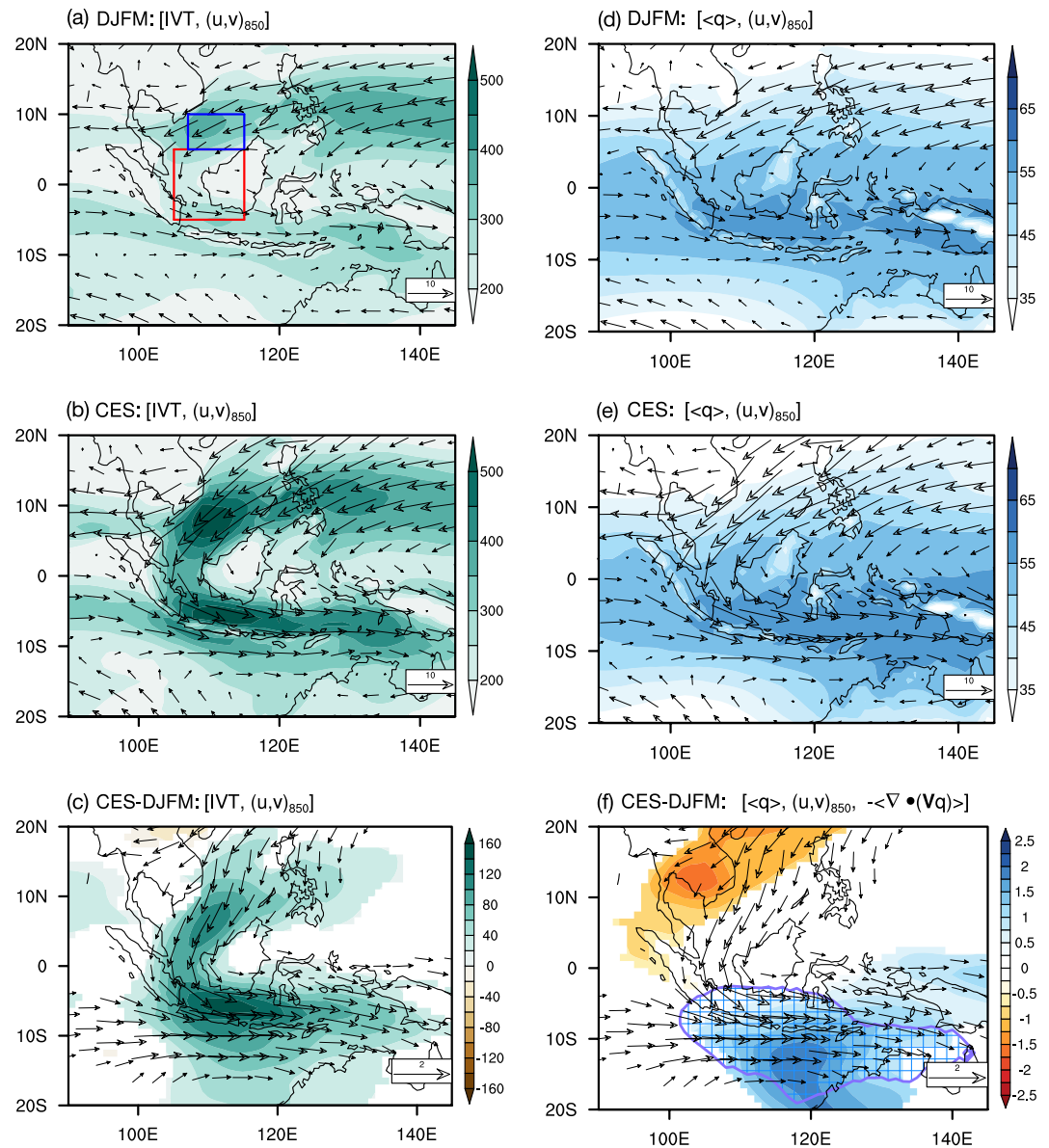


**Figure 1.** (a)–(c) The vertically integrated water vapor transport (IVT;  $\text{kg m}^{-1} \text{s}^{-1}$ , shaded) overlaid with 850 hPa wind ( $\text{m s}^{-1}$ , vectors) over the South China Sea and the MC according to (a) the DJFM climatological mean, (b) the composite analysis of the CES events, (c) the composite anomaly of the CES events from the winter mean. (d)–(f) As in (a)–(c), but for the vertically integrated water vapor ( $\langle q \rangle$ ;  $\text{kg m}^{-2}$ , shaded). Only values that are statistically significant at the 95% confidence level using a bootstrap test are plotted in (c) and (f). The hatched area in (f) denote the vertically integrated moisture flux convergence ( $-\langle \nabla \cdot (\mathbf{V}q) \rangle$ ) greater than  $2 \text{ kg m}^{-2} \text{ day}^{-1}$ .

This resampling is repeated 1,000 times to generate 1,000 composites of MJO\_noCES. We then calculate the mean, minimum, and maximum values of those composites to obtain the spread (i.e., uncertainty) of the composite mean in MJO\_noCES.

### 3. Results

#### 3.1. Large-Scale Conditions Associated With the CES

Before exploring the impacts of the CES on the MJO's southward detour, we first compare the composite mean large-scale conditions (e.g., lower-level winds, column moisture transport, and column water vapor) during CES

events to the climatological mean in DJFM (Figure 1). It is evident that the lower-level (850 hPa) northeasterlies over the wide area of the South China Sea and northwesterlies over the Java Sea strengthens in the presence the CES. This is attributed to the enhanced meridional temperature gradient between high and low latitudes during the CES event (not shown), which in turn facilitates greater moisture vapor transport from the South China Sea to the tropics (Figures 1a–1c). Due to the diabatic warming effect (i.e., warm surfaces and condensational heating), the initially dry and cold surge airflow undergoes a transition into a warmer and more moist state as it enters the tropics, which then penetrates far to the SMC (Figures 1d–1f). The resulting increase in column moisture over the SMC is characterized by positive total moisture flux convergence anomalies, indicative of positive net precipitation (Figure 1f). This finding is consistent with previous studies, showing that cold surges can propagate deep into the tropics, triggering convection and precipitation, which eventually lead to heavy rainfall and flood events (Hattori et al., 2011; Lim et al., 2017; Wu et al., 2013; Xavier et al., 2020; Yulihastin et al., 2020). In addition, the CES-induced moist environment over the SMC suggests its potential role in providing additional moisture and energy for the intensification and propagation of the MJO, which will be investigated in the subsequent section.

### 3.2. Amplification of MJO's Southward Detour by the CES

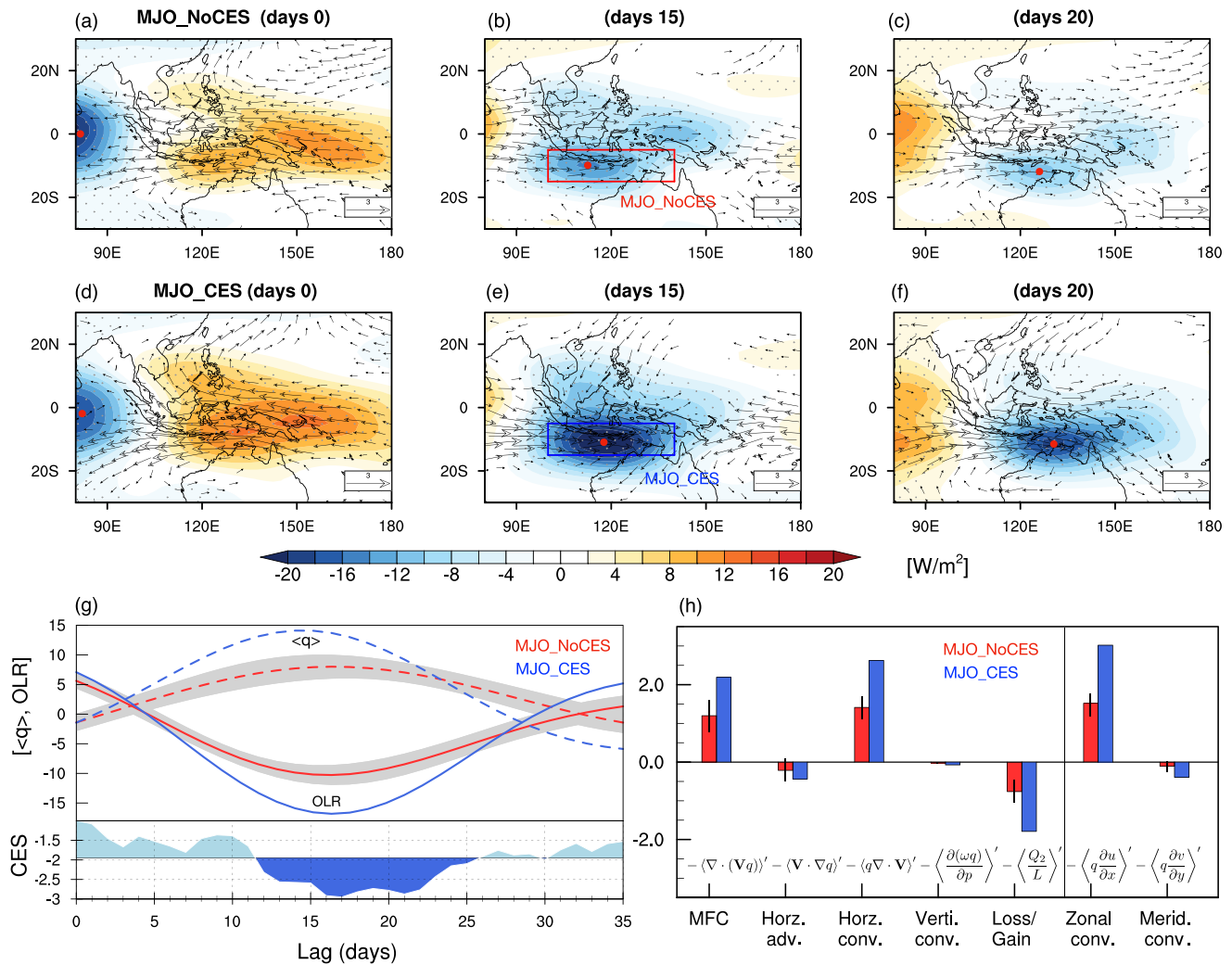
To investigate whether the CES affects MJO over the MC region, we compare MJO events that occur both with and without CES events (Figure 2). Note that through a random sampling procedure, the sample size in MJO\_noCES is equivalent to MJO\_CES to ensure a fair comparison of the composite amplitude (see Section 2.4 for details). In both cases, MJO shows notable variations in its latitudinal structure as it propagates from the Indian Ocean to the MC. Specifically, MJO shifts from a meridionally symmetric structure over the central Indian Ocean (Figures 2a and 2d) to a zonally oriented structure over the MC, consistent with the regions of converging wind anomalies (Figures 2b,c, 2e,f). A marked contrast between MJO\_noCES and MJO\_CES is clearly seen in the amplitude of the southward detour over the SMC, which is noticeably stronger in the presence of a CES compared to when no CES is present. This suggests that the CES has a modulating effect on the strength of the MJO's southward detour over the SMC region.

Figure 2g illustrates the differences in intraseasonal OLR and tropospheric moisture anomalies averaged over the SMC area (15°S–5°S, 100°–140°E, e.g., Kim et al. (2017)) between MJO\_noCES and MJO\_CES events. The comparison reveals that the CES amplifies the intraseasonal OLR and tropospheric moisture anomalies over the SMC region during the MJO event. In particular, at lag days between +5 and +11, when the enhanced convective anomaly propagates toward the central MC, the southward detour becomes gradually stronger in the MJO\_CES, consistent with the onset period of the CES. From lag days +12 to +18, the difference in the MJO amplitude over the SMC between MJO\_CES and MJO\_noCES becomes significantly larger, suggesting that the stronger moisture recharge by the CES leads to more vigorous anomalous convection in the region.

To explore the physical mechanisms through which the CES affects the strength of the MJO's southward detour, we perform a budget analysis for the intraseasonal column-integrated moisture. The analysis of column-integrated moisture budget is motivated by the theoretical framework of the MJO, called the moisture mode theory (Raymond, 2001; Sobel & Maloney, 2013). This theory highlights the close relationship between tropical convection and environmental moisture, assuming a weak temperature gradient in the tropics. The moisture mode theory explains how moisture anomalies are the driving force behind the maintenance and propagation of intraseasonal MJO anomalies. Since the intraseasonal variability of MJO convection is closely tied to column-integrated moisture over the tropics (Figure 2g), the examination of the moisture budget can provide valuable insights into the processes that control the amplitude of the MJO's southward detour.

Figure 2h presents the relative contributions of each moisture budget term to the total moistening process over the SMC during the recharging period (lag days between +8 and +18) for both MJO\_noCES and MJO\_CES events. The result reveals that the increase in horizontal moisture convergence is a key process that is responsible for increasing moisture over the SMC in the presence of the CES (Figure 2h). This increase is primarily attributed to the stronger zonal moisture convergence, which highlights the crucial role of this term in promoting the intensification of the MJO over the SMC during CES events. Furthermore, to better understand how the CES amplifies the zonal moisture convergence, we further examine the respective contributions of the mean state, intraseasonal anomalies, and high-frequency eddy anomalies to the horizontal moisture flux convergence. For this purpose, we focus on the 700 hPa level, where moisture variability is most strongly associated with the MJO (Kim et al., 2017). Note that the results obtained at this specific level are consistent with those obtained through





**Figure 2.** (a)–(c) Composite MJO-filtered OLR (shaded) and 850 hPa wind (vectors) anomalies without CES events (MJO\_noCES) on (a) day 0, (b) day +15 and (c) day +20. (d)–(f) As in (a)–(c), but with CES events (MJO\_CES). Red dots indicate the center of convective anomalies (local minimum of OLR). Black dots denote statistically significant values at the 95% confidence level using a bootstrap test. (g) MJO-filtered column-integrated specific humidity ( $\times 0.2 \text{ kg kg}^{-1}$ , dashed lines), and OLR ( $\text{W m}^{-2}$ , solid lines) anomalies averaged over the SMC area (the box in (b) and (e)). The color red (blue) denotes the MJO\_noCES (MJO\_CES). The gray shading indicates the minimum and maximum values of the composite mean in MJO\_noCES by random resampling (see Section 2 for details). The sub-panel plot shows the composite of the CES index (see text for definition) during the MJO\_CES, with values below 1 standard deviation colored with dark blue. (h) Column-integrated moisture budget ( $\text{kg m}^{-2} \text{ day}^{-1}$ ) averaged over the recharging period (lag days between +8 and +18). The red and blue bar represents the SMC in MJO\_noCES and MJO\_CES, respectively. The two rightmost bars represent the contribution of zonal and meridional terms to the horizontal moisture flux convergence. The vertical black line on the red bars indicates the minimum and maximum values of the composite mean by random resampling.

the column-integrated analysis (see Figure S3 in Supporting Information S1). A closer inspection of the horizontal moisture convergence terms reveals that the zonal convergence by intraseasonal zonal wind anomalies acting upon background moisture is the dominant contribution to the zonal moisture convergence term (Figure 3a). Other terms—such as the high-frequency zonal wind anomaly interacting with the background moisture and the intraseasonal zonal wind anomaly interacting with intraseasonal moisture anomaly—only play a secondary role in contributing to the positive zonal moisture convergence. In addition, we also observe that the high-frequency component of the CES has a non-negligible effect on the meridional moisture convergence (Figure 3b). However, this effect is largely offset by the intraseasonal meridional wind anomalies acting on the climatological moisture.

To further investigate why the zonal convergence by intraseasonal zonal wind acting upon the background moisture process is intensified during CES events, we examine the spatial distribution of the background moisture and intraseasonal wind anomalies (Figures 3c and 3d). Our analysis reveals that the intraseasonal westerly winds

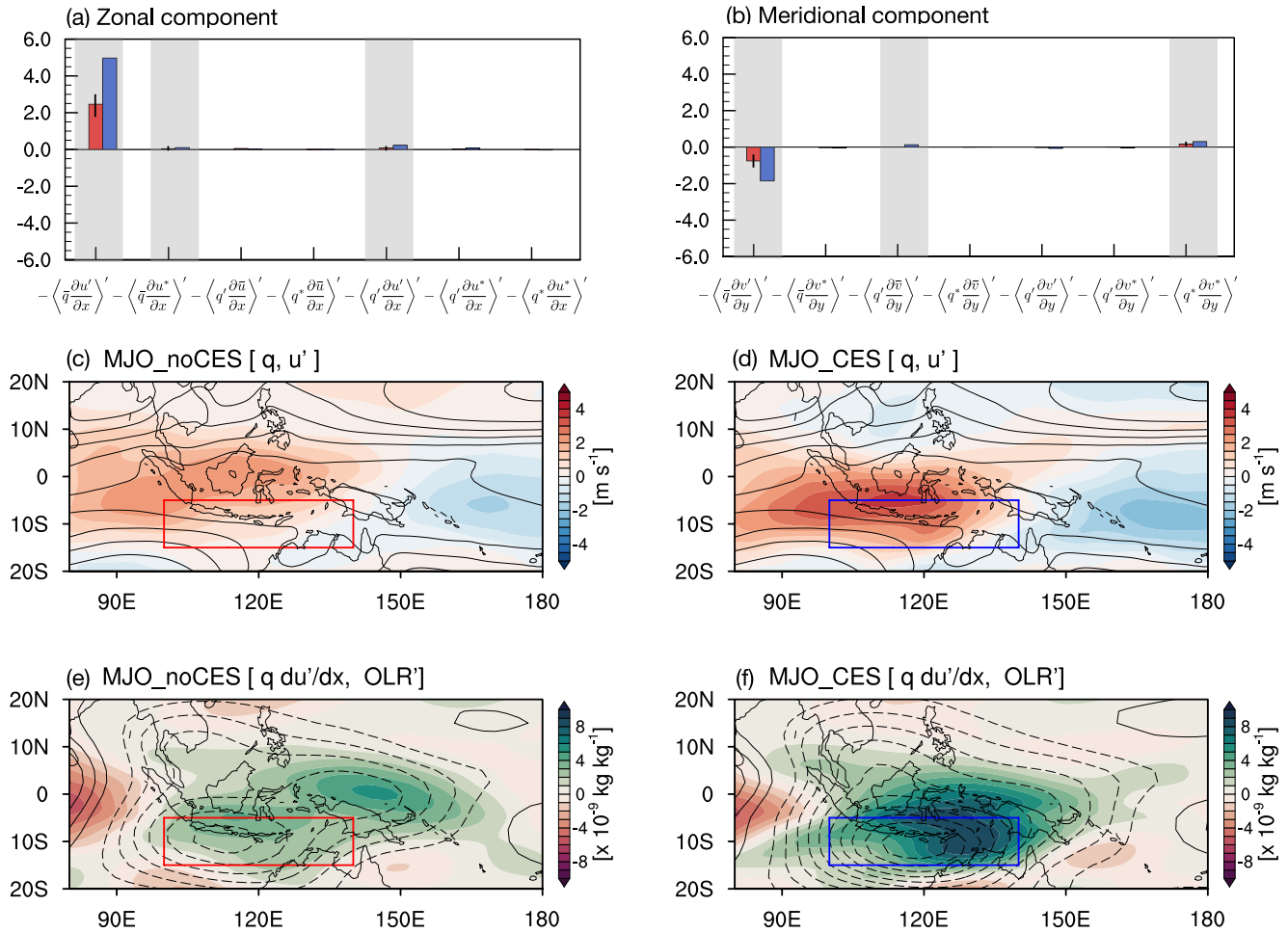


**Figure 3.** (a) Decompositions of the zonal convergence of moisture ( $\times 10^{-9} \text{ kg kg}^{-1} \text{ s}^{-1}$ ) into contribution of the background flow, intraseasonal and high-frequency eddy components. (b) As in (a), but for the meridional component of the horizontal moisture flux convergence. The gray shadings indicate the three most dominant contributors of the zonal/meridional moisture flux convergence. (c)–(d) Intraseasonal zonal wind anomaly ( $\text{m s}^{-1}$ , shaded) averaged over the recharging period (lag days between +8 and +18 at 700 hPa) for (c) MJO\_noCES and (d) MJO\_CES events. The contour lines in (c)–(d) denote the DJFM climatological mean of specific humidity ( $\text{kg kg}^{-1}$ , from  $-10$  to  $10$  with interval of  $1$ ). (e)–(f) Intraseasonal OLR ( $\text{W m}^{-2}$ , contour line from  $-5$  to  $5$ , with interval of  $0.5$ ) and zonal convergence by intraseasonal zonal wind anomalies acting upon background moisture ( $\times 10^{-9} \text{ kg kg}^{-1} \text{ s}^{-1}$ , shaded) during the recharging period for (e) MJO\_noCES and (f) MJO\_CES events. The rectangle in each panel indicates the southern MC area.

becomes significantly stronger over the SMC regions in the presence of the CES (Figures 3c and 3d). Note that the mean-state zonal wind in DJFM is westerly (not shown). This strengthening is consistent with the nature of the CES, which exhibits intraseasonal variations, particularly when it crosses the equator (as shown in our Figures S1 and S2 in Supporting Information S1 and confirmed by Lim et al. (2017), Xavier et al. (2020)). This condition, in turn, enhances the zonal moisture convergence over the SMC (Figure 3f). As the background moisture during this period is associated with the Australian monsoon system, this indicates that the background moisture during the active monsoon season helps increase the zonal moisture flux convergence during the CES events. In contrast, in the absence of CES events, the peak of intraseasonal wind anomalies is more localized over the equator and considerably weaker over the SMC region (Figure 3c), resulting in substantially weaker zonal moisture convergence over the SMC (Figure 3e).

### 3.3. CES-Induced Strengthening of Wind-Evaporation Feedback

Given the observed relationship between stronger zonal moisture convergence and intraseasonal wind intensification during CES events, one intriguing question arises: Could the amplification of the MJO southward detour be attributed to stronger wind-evaporation feedback in the presence of the CES? The wind-evaporation feedback,

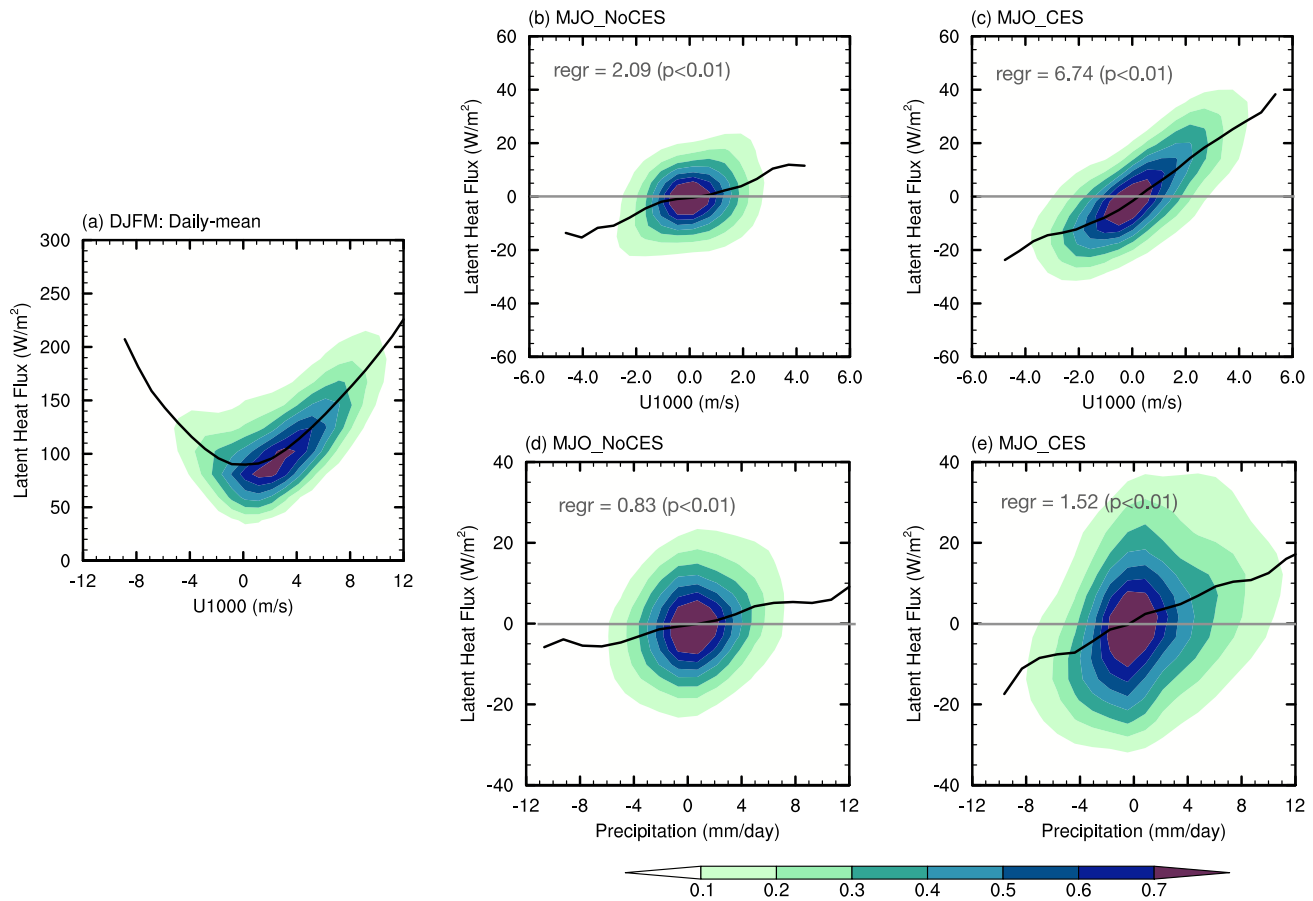


**Figure 4.** (a) Joint histogram of daily zonal wind at 1,000 hPa ( $\text{m s}^{-1}$ ; x axis) and surface latent heat flux ( $\text{W m}^{-2}$ ; y axis) collected over the ocean grid points in the SMC region ( $15^{\circ}$ – $5^{\circ}$ S,  $110^{\circ}$ – $140^{\circ}$ E). (b)–(c) As in (a), but for MJO-filtered anomalies without the CES (MJO\_noCES) and with the CES (MJO\_CES). (d)–(e) As in (b)–(c), but for the joint histogram of MJO-filtered precipitation anomaly ( $\text{mm day}^{-1}$ ; x axis) and the MJO-filtered surface latent heat flux anomaly ( $\text{W m}^{-2}$ ; y axis). Black solid lines indicate averaged latent heat flux values onto zonal wind bins (a)–(c) and onto precipitation bins (d)–(e). Results with fewer than 100 samples are omitted. Regression coefficients of average latent heat flux values to zonal wind bins (a)–(c) and to precipitation bins (d)–(e) are indicated in the panel, and the  $p$ -value in the parenthesis indicates significance of the regression coefficient difference from DJFM. All joint histograms in (b)–(e) are calculated from lag 0 to lag +25 (the period during which the MJO is located over the MC).

also known as wind-induced surface heat exchange, is a crucial process in the propagation and maintenance of the MJO (Bui & Maloney, 2020; Kang et al., 2022; Maloney & Sobel, 2004). Here, we hypothesize that the stronger westerlies in the presence of the CES can result in a stronger surface latent heat flux, leading to more moisture being supplied to the atmosphere over the SMC. This condition, in turn, could contribute to the amplification of the MJO southward detour.

Figure 4a shows the joint histogram of daily near-surface zonal wind and surface latent heat flux over the SMC region during DJFM. As expected, higher values of latent heat flux are associated with stronger zonal winds. Note that the zonal wind is the primary contributor to total wind speed over this region (Figure 1a). A comparison of the joint histogram of the MJO anomalies between MJO\_noCES and MJO\_CES during the period of MJO propagation over the ocean grid points in the MC region (from lag 0 to lag +25) (Figures 4b and 4c) indicates that a much steeper slope of the average latent heat flux is observed in the presence of the CES, which suggests a stronger relationship between latent heat flux and zonal wind speed (i.e., stronger feedback). This relationship implies that, during CES events, the same amount of MJO wind anomaly corresponds to a much greater latent heat flux anomaly (i.e., a higher rate of water evaporation from the surface to the atmosphere). This notion is supported by the positive correlation between precipitation and latent heat flux anomalies, with a steeper slope during CES events (Figures 4d and 4e). The stronger positive feedback between precipitation and latent heat flux anomalies suggests that the CES enhances the wind-evaporation feedback under a moisture mode paradigm, thus contributing to the stronger MJO convection over the SMC.





amplitude over the Indian Ocean. Therefore, it is clear that the MJO's amplitude is not entirely suppressed during the CES; rather, it undergoes a shift and amplification toward the SMC due to enhanced convection (see the illustration in Figure 5).

This study improves our understanding of the dynamics that govern the intensity and propagation of the MJO over the MC, which can ultimately improve our ability to forecast and mitigate the impacts of extreme weather events in the affected regions (Wu et al., 2013; Lubis et al., 2022). Furthermore, the diagnostics developed in this study can be useful for investigating the processes that lead to the moisture and circulation biases in simulating MJO in climate models or operational forecast models (e.g., Li et al., 2017), with an emphasis on the role of extratropical-tropical interaction through the CES. While our study does not consider other important processes over the MC, such as the diurnal cycle of convection over the islands (Hagos et al., 2016), the Borneo vortex (Chang et al., 2005), or the potential role of more rotational types of convectively coupled equatorial waves (Diong et al., 2023; Latos et al., 2021; Lubis & Jacobi, 2015), further investigations into these processes may also be necessary to fully explain the dynamics of the MJO and CES interaction. These topics can be fruitful directions for future research.

## Data Availability Statement

All data used in this manuscript are publicly available. The ERA-5 reanalysis data are publicly available at <https://www.ecmwf.int/en/forecasts/dataset/ecmwf-reanalysis-v5>. The NASA GPM data can be obtained from <https://doi.org/10.5067/GPM/IMERGDF/DAY/06>. The OLR data was obtained from <https://psl.noaa.gov/data/gridded/data.olrdr.interp.html>. The moisture budget codes are available from <https://doi.org/10.5281/zenodo.8128964>.

## References

- Abdillah, M. R., Kanno, Y., Iwasaki, T., & Matsumoto, J. (2021). Cold surge pathways in East Asia and their tropical impacts. *Journal of Climate*, 34(1), 157–170. <https://doi.org/10.1175/JCLI-D-20-0552.1>
- Bui, H. X., & Maloney, E. D. (2020). Changes to the Madden-Julian oscillation in coupled and uncoupled aquaplanet simulations with 4xCO<sub>2</sub>. *Journal of Advances in Modeling Earth Systems*, 12(8), e2020MS002179. <https://doi.org/10.1029/2020MS002179>
- Chang, C.-P., Harr, P. A., & Chen, H.-J. (2005). Synoptic disturbances over the equatorial South China Sea and western maritime continent during boreal winter. *Monthly Weather Review*, 133(3), 489–503. <https://doi.org/10.1175/MWR-2868.1>
- Diong, J.-Y., Xavier, P., Woolnough, S. J., & Abdullah, F. A. (2023). Equatorial Rossby waves on cold surge days and their impact on rainfall. *Quarterly Journal of the Royal Meteorological Society*. <https://doi.org/10.1002/qj.4493>
- Efron, B. (1979). Bootstrap methods: Another look at the jackknife. *Annals of Statistics*, 7(1), 1–26. <https://doi.org/10.1214/aos/1176344552>
- Hagos, S., Zhang, C., Feng, Z., Burleyson, C. D., De Mott, C., Kerns, B., et al. (2016). The impact of the diurnal cycle on the propagation of Madden-Julian oscillation convection across the maritime continent. *Journal of Advances in Modeling Earth Systems*, 8(4), 1552–1564. <https://doi.org/10.1002/2016MS000725>
- Hattori, M., Mori, S., & Matsumoto, J. (2011). The cross-equatorial northerly surge over the maritime continent and its relationship to precipitation patterns. *Journal of the Meteorological Society of Japan. Ser. II*, 89A, 27–47. <https://doi.org/10.2151/jmsj.2011-A02>
- Hersbach, H., Bell, B., Berrisford, P., Hirahara, S., Horányi, A., Muñoz-Sabater, J., et al. (2020). The ERA5 global reanalysis. *Quarterly Journal of the Royal Meteorological Society*, 146(730), 1999–2049. <https://doi.org/10.1002/qj.3803>
- Hsu, P.-C., & Li, T. (2012). Role of the boundary layer moisture asymmetry in causing the eastward propagation of the Madden-Julian oscillation. *Journal of Climate*, 25(14), 4914–4931. <https://doi.org/10.1175/JCLI-D-11-00310.1>
- Huffman, G. J., Bolvin, D. T., Braithwaite, D., Hsu, K.-L., Joyce, R. J., Kidd, C., et al. (2020). Integrated multi-satellite retrievals for the global precipitation measurement (GPM) mission (IMERG). In *Satellite precipitation measurement* (pp. 343–353). Springer.
- Kang, D., Kim, D., Ahn, M.-S., & An, S.-I. (2021). The role of the background meridional moisture gradient on the propagation of the MJO over the maritime continent. *Journal of Climate*, 34(16), 6565–6581. <https://doi.org/10.1175/JCLI-D-20-0085.1>
- Kang, D., Kim, D., Rushley, S., & Maloney, E. (2022). Seasonal locking of the MJO's southward detour of the maritime continent: The role of the Australian monsoon. *Journal of Climate*, 35(24), 8153–8168. <https://doi.org/10.1175/JCLI-D-22-0234.1>
- Kim, D., Kim, H., & Lee, M.-I. (2017). Why does the MJO detour the maritime continent during austral summer? *Geophysical Research Letters*, 44(5), 2579–2587. <https://doi.org/10.1002/2017GL072643>
- Latos, B., Lefort, T., Flatau, M. K., Flatau, P. J., Permana, D. S., Baranowski, D. B., et al. (2021). Equatorial waves triggering extreme rainfall and floods in southwest Sulawesi, Indonesia. *Monthly Weather Review*, 149(5), 1381–1401. <https://doi.org/10.1175/mwr-d-20-0262.1>
- Li, Q., Yang, S., Wu, T., & Liu, X. (2017). Subseasonal dynamical prediction of East Asian cold surges. *Weather and Forecasting*, 32(4), 1675–1694. <https://doi.org/10.1175/WAF-D-16-0209.1>
- Liebmann, B., & Smith, C. A. (1996). Description of a complete (interpolated) outgoing longwave radiation dataset. *Bulletin of the American Meteorological Society*, 77(6), 1275–1277.
- Lim, S. Y., Marzin, C., Xavier, P., Chang, C.-P., & Timbal, B. (2017). Impacts of boreal winter monsoon cold surges and the interaction with MJO on Southeast Asia rainfall. *Journal of Climate*, 30(11), 4267–4281. <https://doi.org/10.1175/JCLI-D-16-0546.1>
- Lubis, S. W., Hagos, S., Hermawan, E., Respati, M. R., Ridho, A., Risyanto, et al. (2022). Record-breaking precipitation in Indonesia's capital of Jakarta in early January 2020 linked to the northerly surge, equatorial waves, and MJO. *Geophysical Research Letters*, 49(22), e2022GL101513. <https://doi.org/10.1029/2022GL101513>
- Lubis, S. W., & Jacobi, C. (2015). The modulating influence of convectively coupled equatorial waves (CCEWS) on the variability of tropical precipitation. *International Journal of Climatology*, 35(7), 1465–1483. <https://doi.org/10.1002/joc.4069>

## Acknowledgments

This work is supported by U.S. Department of Energy Office of Science Biological and Environmental Research as part of Global and Regional Model Analysis program area. Computing resources for the analysis are provided by the National Energy Research Scientific Computing Center (NERSC), a DOE Office of Science User Facility supported by the Office of Science of the U.S. Department of Energy under Contract No. DE-AC02-05CH11231. Pacific Northwest National Laboratory is operated by Battelle for the U.S. Department of Energy under Contract DE-AC05-76RLO1830.

- Maloney, E. D., & Sobel, A. H. (2004). Surface fluxes and ocean coupling in the tropical intraseasonal oscillation. *Journal of Climate*, 17(22), 4368–4386. <https://doi.org/10.1175/JCLI-3212.1>
- Pang, B., Lu, R., & Ling, J. (2018). Impact of cold surges on the Madden-Julian oscillation propagation over the maritime continent. *Atmospheric Science Letters*, 19(10), e854. <https://doi.org/10.1002/asl.854>
- Raymond, D. J. (2001). A new model of the Madden-Julian oscillation. *Journal of the Atmospheric Sciences*, 58(18), 2807–2819. [https://doi.org/10.1175/1520-0469\(2001\)058<2807:ANMOTM>2.0.CO;2](https://doi.org/10.1175/1520-0469(2001)058<2807:ANMOTM>2.0.CO;2)
- Singh, B., & Kinter, J. L. (2020). Tracking of tropical intraseasonal convective anomalies: 1. Seasonality of the tropical intraseasonal oscillations. *Journal of Geophysical Research: Atmospheres*, 125(3), e2019JD030873. <https://doi.org/10.1029/2019JD030873>
- Sobel, A., & Maloney, E. (2013). Moisture modes and the eastward propagation of the MJO. *Journal of the Atmospheric Sciences*, 70(1), 187–192. <https://doi.org/10.1175/JAS-D-12-0189.1>
- Wheeler, M., & Kiladis, G. N. (1999). Convectively coupled equatorial waves: Analysis of clouds and temperature in the wavenumber–frequency domain. *Journal of the Atmospheric Sciences*, 56(3), 374–399. [https://doi.org/10.1175/1520-0469\(1999\)056<0374:CCEWAO>2.0.CO;2](https://doi.org/10.1175/1520-0469(1999)056<0374:CCEWAO>2.0.CO;2)
- Wu, P., Arbain, A. A., Mori, S., Hamada, J.-I., Hattori, M., Syamsudin, F., & Yamanaka, M. D. (2013). The effects of an active phase of the Madden-Julian oscillation on the extreme precipitation event over western java island in January 2013. *Solanus*, 9(0), 79–83. <https://doi.org/10.2151/sola.2013-018>
- Wu, P., Hara, M., Fudeyasu, H., Yamanaka, M. D., Matsumoto, J., Syamsudin, F., et al. (2007). The impact of trans-equatorial monsoon flow on the formation of repeated torrential rains over Java Island. *Solanus*, 3, 93–96. <https://doi.org/10.2151/sola.2007-024>
- Xavier, P., Lim, S. Y., Ammar Bin Abdullah, M. F., Bala, M., Chenoli, S. N., Handayani, A. S., et al. (2020). Seasonal dependence of cold surges and their interaction with the Madden-Julian oscillation over Southeast Asia. *Journal of Climate*, 33(6), 2467–2482. <https://doi.org/10.1175/jcli-d-19-0048.1>
- Yulihastin, E., Wahyu Hadi, T., Sari Ningsih, N., & Ridho Syahputra, M. (2020). Early morning peaks in the diurnal cycle of precipitation over the northern coast of west java and possible influencing factors. *Annales Geophysicae*, 38(1), 231–242. <https://doi.org/10.5194/angeo-38-231-2020>
- Zhang, C., & Dong, M. (2004). Seasonality in the Madden-Julian oscillation. *Journal of Climate*, 17(16), 3169–3180. [https://doi.org/10.1175/1520-0442\(2004\)017<3169:SITMO>2.0.CO;2](https://doi.org/10.1175/1520-0442(2004)017<3169:SITMO>2.0.CO;2)
- Zhou, L., & Murtugudde, R. (2020). Oceanic impacts on MJOs detouring near the maritime continent. *Journal of Climate*, 33(6), 2371–2388. <https://doi.org/10.1175/JCLI-D-19-0505.1>

## Erratum

In the originally published version of this article, the heading for Section 4 was published incorrectly as “Summary and Conclusion” in place of “Summary and Discussion.” The error has been corrected, and this may be considered the authoritative version of record.